

# Semicoherent Symmetric Quantum Processes: Theory and Applications

Yan Wang,<sup>1,\*</sup> Sarah Chehade,<sup>1,†</sup> and Eugene Dumitrescu<sup>1,‡</sup>

<sup>1</sup>*Computational Sciences and Engineering Division,  
Oak Ridge National Laboratory, Oak Ridge, Tennessee 37831, USA*

(Dated: March 11, 2024)

Discovering pragmatic and efficient approaches to synthesize  $\varepsilon$ -approximations to quantum operators such as real (imaginary) time-evolution propagators in terms of the basic quantum operations (gates) is challenging. These invaluable  $\varepsilon$ -approximations enable the compilation of classical and quantum algorithms modeling, e.g., dynamical properties. In parallel, symmetries are powerful tools concisely describing the fundamental laws of nature; the symmetrical underpinnings of physical laws having consistently provided profound insights and substantially increased predictive power. In this work, we consider the interplay between  $\varepsilon$ -approximations processes and symmetries in a semi-coherent context—where measurements occur at each logical clock cycle. We draw inspiration from Pascual Jordan’s groundbreaking formulation of non-associative, but commutative, algebraic forms. Our symmetrized formalism is applied in various domains such as quantum random walks, real-time-evolutions, variational algorithms ansatzes, and efficient entanglement verification. Our work paves the way for a deeper understanding and greater appreciation of how symmetries can be used to control quantum dynamics in the near-term.

## I. INTRODUCTION

Block encoded quantum operators enable linear combination of unitaries (LCU) [1], as well as  $\mathfrak{su}(2)$  [2] and  $\mathfrak{su}(1,1)$  [3] quantum signal processing. They also facilitate the generalizations of  $\mathfrak{su}(2)$  qubitization [4], and more recently, simulations of open quantum dynamics [5, 6]. Numerous optimizations of these algorithms exist [7–10]. When used in a *fully coherent* manner, quantum resources offer theoretical gold-standard speedups with respect to precision scalings [11]. However, the resources necessary to dynamically evolve the system over long time scales in a fully coherent manner are not currently available in present or near-term quantum devices. This motivates us to take a more pragmatic approach and ask: what applications are realizable with more near-term *semi-coherent* quantum dynamics due to quantum channels with interleaved unitaries and measurement operations?

Hale Trotter’s operator splitting decomposition method [12, 13] for approximating non-commutative semi-group dynamics is a natural starting choice for integrating the unitary Lie group dynamics of the

Schrödinger equation  $i\hbar \frac{\partial}{\partial t} |\Psi(t)\rangle = H |\Psi(t)\rangle$  and factorizing the non-unitary thermal density operator  $e^{-H/(k_B T)}$  for imaginary time evolutions. In both cases, the Hamiltonian operator  $H$  can be split into at least two terms  $H = H_A + H_B$ , where the *individual* factors  $H_A$  and  $H_B$  can be exactly or efficiently exponentiated. In fact, the study of Trotter factorization errors [14] has continued to grow like Hilbert spaces: exponentially. Hence, it is desirable to develop an analytical theory for Trotter formulas and optimize them with regards to precision and cost. This applies to applications in both classical and quantum computing [10, 15–17]. Throughout these studies, Trotter formulas exhibit a time-reversal inversion symmetric (TRIS) partner  $U(-t)$  such that  $U(-t)U(t) = \mathbb{1}$ , which corresponds to the approximate integrator  $U(t)$ , formulated by Suzuki [18].

In this work, we apply symmetrical forms<sup>1</sup> that combine important features of block encodings and algebraic symmetries to quantum processes spanning from dynamics to entanglement verification. This work is organized as follows. Section II defines the algebraic methodologies, culminating Eq. (7), which is the generator of the *symmetry gadget* depicted by the quantum circuit in Fig. 1. The symmetry gadget can be concatenated in iterative algorithms even though the Jordan product  $\circ$ , on which the gadget is based, is non-associative. In Sec. III, we adapt our protocol for a variety of quantum computing applications through variations of the symmetry gadget. First, we synthesize symmetrized non-unitary time-evolution operators, such as  $\frac{1}{2}(e^{-itH} \pm e^{+itH})$ , to naturally encode semi-coherent symmetric quantum walks (Sec. III A). Through projective measurements, the gad-

---

This manuscript has been authored by UT-Battelle, LLC, under Contract No. DE-AC0500OR22725 with the U.S. Department of Energy. The United States Government retains and the publisher, by accepting the article for publication, acknowledges that the United States Government retains a non-exclusive, paid-up, irrevocable, worldwide license to publish or reproduce the published form of this manuscript, or allow others to do so, for the United States Government purposes. The Department of Energy will provide public access to these results of federally sponsored research in accordance with the DOE Public Access Plan.

\* wany2@ornl.gov

† chehades@ornl.gov

‡ dumitrescuef@ornl.gov

---

<sup>1</sup> This includes both symmetry and anti-symmetry, with +1 and -1 eigenvalue, respectively.

get steers the quantum state to eigenstates of the control Hamiltonian since they are the absorbing states of the symmetrical-walk and thus can be used to prepare eigenstates. Next, we propose a second-order Trotter form given by the *commutative* Jordan product [19]:  $e^{itH_A} \circ e^{itH_B} \equiv (e^{itH_A} e^{itH_B} + e^{itH_B} e^{itH_A})/2$  (Sec. III B). By preserving the algebraic inversion symmetry  $A \leftrightarrow B$  of the  $A$  and  $B$  sub-parts (sub-lattices) we show systematic improvements in factorizations of random and deterministic dynamics and also in variational ansatz convergence (Sec. III C). Reducing the measurement complexity of entanglement verification protocols is the last application presented in Sec. III D before a concluding discussion in Sec. IV.

## II. EXCHANGE FACTORIZATION

### A. Higher-Order Precision Extrapolation

To simplify notation we write  $H = A + B$ . To then approximate the global integrator (over the time-path parameter  $t \in \mathbb{R}$ ), with split-term integrators  $e^{tA}$  and  $e^{tB}$ , the first order Trotter formula reads  $e^{tH} \approx e^{tA} e^{tB} + \mathcal{O}(t^2[A, B])$  or  $e^{tB} e^{tA} + \mathcal{O}(t^2[A, B])$ . To synthesize more accurate approximations one idea is to combine counter-driving terms that destructively interfere with the error contributions at leading orders in the operator expansion.

Additional time evolution terms can be introduced at the end of full time evolution path or sandwiched between fractional points of the path, in either additive or multiplicative forms to eliminate leading order commutators. For example, the well-known Zassenhaus formula [20] adds a multiplicative correction to the end of the path, whereas Lie-Trotter-Suzuki formulas [18] incorporate multiplicative correction throughout a fractal path. Therefore, to increase the order of the Trotter-formula and simultaneously reduce fluctuations from truncated higher order which contribute to the overall error norm, we investigate symmetrizing across  $A$  and  $B$  using an additive (commutator) form  $(e^{tA} e^{tB} + (-) e^{tB} e^{tA})/2$ . The proposed methods are detailed in the investigation below.

The Baker-Campbell-Hausdorff (BCH) formula is a formal Lie series solution to  $z$  in the equation  $e^A e^B = e^{z(A, B)}$ , where  $A$  and  $B$  do not necessarily commute.

Given  $(e^{-A} e^{-B})^{-1} = e^B e^A$  implies that  $[e^{z(-A, -B)}]^{-1} = e^{-z(-A, -B)} = e^{z(B, A)}$ , an algebraic symmetry of the BCH series expansion exists:  $z(B, A) = -z(-A, -B)$ . This symmetry manifests as a combination of time-reversal and inversion symmetry (TRIS), expressed by the equation:

$$z(tB, tA) = -z((-t)A, (-t)B),$$

whenever a time variable  $t$  is explicitly introduced. Note that the BCH formula is not symmetric under either time-reversal (TR) or inversion (I) individually but only under the product TRIS.

The Lieb-Robinson-Haah [15] construction utilizes backward time evolution, minimizing errors. Backward-time evolution is also essential in Lie-Trotter-Suzuki formulas, as highlighted in Theorem 3 in Ref. [18], except for the first and second order Trotter formulas. In examples involving LCU, certain coefficients within the linear combination must be negative [1]. This introduces instability in the success probability of the unitary approximations.

If we express  $z(A, B)$  as  $z(A, B) = \sum_{n=1}^{\infty} z_n(A, B)$ , where  $z_n(A, B)$  represents a homogeneous degree- $n$  polynomial of  $A$  and  $B$ , expressed in terms of  $(n-1)$ -level nested commutators of  $A$  and  $B$ , we can derive some key relationships. Specifically, the sum of the odd-degree terms of the expansion, denoted as  $z_{\text{odd}}(A, B) = \sum_{\text{odd } n} z_n(A, B)$ , satisfies  $z_{\text{odd}}(A, B) = z_{\text{odd}}(B, A)$  due to the I-symmetry  $z_n(A, B) = z_n(B, A)$  for odd  $n$ . Meanwhile, the sum of the even-degree terms, denoted as  $z_{\text{even}}(A, B)$ , fulfills an inversion anti-symmetry  $z_{\text{even}}(A, B) = -z_{\text{even}}(B, A)$ , as a consequence of  $z_n(A, B) = -z_n(B, A)$  for even  $n$ . The algebraic symmetry  $z_n(A, B) = (-1)^{n-1} z_n(B, A)$  is part of Theorem 1 in Goldberg's work [21]. Another way to see this is to explicitly pull out the Abelian time-path  $-t$  factor; noting the TRIS must also hold for every order of  $t^n$ . That is  $z_n(B, A)t^n = z_n(tB, tA) = -z_n((-t)A, (-t)B) = -(-t)^n z_n(A, B) = (-1)^{n-1} z_n(A, B)t^n$ , so that  $z_n(A, B) = (-1)^{n-1} z_n(B, A)$ . Finally, for every Trotter evolution  $e^{tB} e^{tA}$  (with Zassenhaus generator  $z(A, B)$ ), its time-reversal conjugate is the expected hermitian conjugate  $e^{-tA} e^{-tB}$  (with Zassenhaus generator  $z(-B, -A)$ ) obeying the TRIS  $z(-B, -A) + z(A, B) = 0$ .

$$z(A, B) \equiv A \blacklozenge B \equiv \log(e^A e^B) \tag{1}$$

$$= (A + B) + \frac{1}{2}[A, B] + \frac{1}{12}([A, [A, B]] + [B, [B, A]]) + \frac{1}{24}[A, [B, [B, A]]] + \dots \tag{2}$$

$$\equiv z_1(A, B) + z_2(A, B) + z_3(A, B) + z_4(A, B) + \dots \tag{3}$$

$$= \sum_{\text{odd } n > 0} z_n(A, B) + \sum_{\text{even } n > 0} z_n(A, B) \equiv z_{\text{odd}}(A, B) + z_{\text{even}}(A, B), \tag{4}$$

where the binary product “ $\blacklozenge$ ” is borrowed from Ref. 22 (p115) with  $z_1(A, B) = A + B$ ,  $z_2(A, B) = \frac{1}{2}(AB - BA)$ ,  $z_3(A, B) = \frac{1}{12}(A^2B + BA^2 + B^2A + AB^2 - 2ABA - 2BAB)$ ,  $z_4(A, B) = \frac{1}{24}(A^2B^2 - B^2A^2 - 2ABAB + 2BABA)$ , etc. The term  $z_n(A, B)$  is uniquely expressed in the form of polynomials but the commutator form is not unique due to Jacobi identity of the Lie algebra. In the above, rearranging the odd-degree and even-degree terms into two sums implies the assumption that the original series is absolutely convergent.

Let us move on to consider the symmetric Jordan-Trotter product form, defined as the symmetrized product (denoted as “ $\circ$ ”) within an *associative* algebra  $(\mathcal{A}, \cdot)$

For any  $U, V \in \mathcal{A}$ , the not necessarily associative, but *commutative*,  $\circ$  operation between  $U$  and  $V$  is defined as

$$U \circ V := \frac{1}{2}\{U, V\} \equiv \frac{1}{2}(UV + VU). \quad (5)$$

The above defines a *special* Jordan algebra  $(\mathcal{A}^+, \circ)$ . (If  $\mathcal{A}$  is non-associative, the above defines an exceptional Jordan algebra.) This symmetric-Jordan-Trotter product form is a tool to expand the order of a Trotter sequence from  $2p$  to  $2p + 1$ , taking the error from  $\mathcal{O}(t^{2p+1}) \rightarrow \mathcal{O}(t^{2p+2})$ . Specifically, we begin with a first order sequence and analytically eliminate the first order synthesis error. For example,  $e^{A+B} \approx e^{z_+(A, B)}$ , where

$$z_+(A, B) = \log(e^A \circ e^B) \equiv \log \left[ \frac{1}{2}(e^A e^B + e^B e^A) \right] \quad (6)$$

$$= (A + B) + \frac{1}{12}([A, [A, B]] + [B, [B, A]]) + \frac{1}{8}[A, B]^2 + \dots, \quad (7)$$

which can be compared with

$$z_{\text{odd}}(A, B) = A \circ_{\blacklozenge} B \equiv \frac{1}{2}(A \blacklozenge B + B \blacklozenge A) \quad (8)$$

$$= \frac{1}{2}[z(A, B) + z(B, A)] \quad (9)$$

$$= \frac{1}{2}[\log(e^A e^B) + \log(e^B e^A)] \quad (10)$$

$$= (A + B) + \frac{1}{12}([A, [A, B]] + [B, [B, A]]) + \dots, \quad (11)$$

where “ $\circ_{\blacklozenge}$ ” denotes a special Jordan algebra derived from the  $\blacklozenge$  product.

Eq. (11) only has odd degree terms, so the first term omitted in the ellipse is the degree-5 term. Eqs. (7) and (11) agree up to the degree-3 terms. In Eq. (7), the coefficient of degree-4 term is not a nested commutator. This is because  $[A, B]^2$  does not belong to the free Lie algebra, as indicated by the criterion in the Dynkin-Specht-Wever Lemma/Theorem [22, 23]. However, for a given representation, such as the defining matrix representation of the Lie algebra, it is possible that  $[A, B]^2$  can be written as a Lie algebra element or even nested commutators only involving  $A$  and  $B$  (consider the Pauli matrix representation of  $\mathfrak{su}(2)$  as an example). Due to the commutativity of the Jordan product, Eq. (7) has the symmetry  $z_+(A, B) = z_+(B, A)$ , while the TRIS is broken at fourth order since  $z_+(A, B) + z_+(-B, -A) = \frac{1}{4}[A, B]^2 \neq 0$  for non-commutative  $A$  and  $B$ . We define

$$U_{\pm}(t) = \frac{1}{2}(e^{tA} e^{tB} \pm e^{tA} e^{tB}). \quad (12)$$

So  $U_+(t) = e^{z_+(t)}$ , but the analogous  $z_-$  is not well defined since  $U_-$  is not close to identity operator as  $t \rightarrow 0$ .

Our discussion so far has been opaque with regards to the implementation details defining how these operators are synthesized on quantum computers. In the next two subsections we consider different implementation and their repercussions regarding BCH expansion synthesis.

We first demonstrate that the gadget in Fig. 1 gives our symmetrized operator. Subsequently, we examine the success probability of each scattering trajectory of the ancilla qubit  $|0\rangle_a \rightarrow |0\rangle_a (|1\rangle_a)$ . These trajectories correspond to the term with the + (−) phase factor in front of  $V$  below. The terms are essentially “kicked back” from the sign of interference matrix elements  $\langle 0|-\rangle\langle -|0\rangle_a$  ( $\langle 1|-\rangle\langle -|0\rangle_a$ ) of the ancilla qubit. Here,  $|\pm\rangle_a = (|0\rangle_a \pm |1\rangle_a)/\sqrt{2}$  are the eigenstates of the  $X_a$  operator, and  $|+\rangle_a = H_a |0\rangle_a$  and  $|-\rangle_a = H_a |1\rangle_a$ , where  $H_a = (X_a + Z_a)/\sqrt{2}$  is the Hadamard gate acting on the ancilla qubit. The following calculation is essentially the same as that for Lemma 2 (specifically  $\kappa = 1$ ) in Ref. [1]. Representing the final measurements as a complete sum of projection operators  $\mathbb{1}_a \otimes \mathbb{1} = |0\rangle\langle 0|_a \otimes \mathbb{1} + |1\rangle\langle 1|_a \otimes \mathbb{1}$  for the initial state  $|0\rangle_a \otimes |\Psi\rangle$ , we show that the gadget performs the unitary transformation as follows.

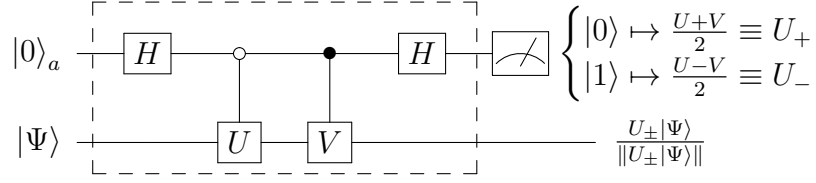


FIG. 1. Selecting  $U = V^\dagger = e^{-itH}$  we define a random spectral walk (Sec. III A). Using  $U = e^{tA}e^{tB}$  and  $V = e^{tB}e^{tA}$ , the quantum circuit acts by the BCH series that is symmetric with respect to  $A \leftrightarrow B$ . This is used to factorize time-evolution (Sec. III B). Setting different times ( $t \rightarrow \theta_1, \theta_2$ ) enables a symmetric variational ansatz (Sec. III C). Last, setting  $U = X_l$  and  $V = iY_l$  for an array of qubits  $\{q_l\}_{l=1}^N$  and concatenating the gadget  $N$ -times performs the measurement of Mermin polynomial  $M_N$  with a linear depth circuit (Sec. III D). The symmetry of the operator applied to  $|\Psi\rangle$  is contingent on a measurement an ancillary qubit in the  $(|1\rangle)$   $|0\rangle$  state. Note that  $U_\pm$  are not unitary and that the principle system's final state  $U_\pm |\Psi\rangle$  is normalized upon measurement of the ancilla qubit, due to the measurement postulate.

$$\begin{aligned}
& \left( |0\rangle\langle 0|_a \otimes \mathbb{1} + |1\rangle\langle 1|_a \otimes \mathbb{1} \right) (H_a \otimes \mathbb{1}) \left( |0\rangle\langle 0|_a \otimes \mathbb{1} + |1\rangle\langle 1|_a \otimes V \right) \left( |0\rangle\langle 0|_a \otimes U + |1\rangle\langle 1|_a \otimes \mathbb{1} \right) (H_a \otimes \mathbb{1}) (|0\rangle_a \otimes |\Psi\rangle) \\
&= \left( |0\rangle\langle 0|_a \otimes \mathbb{1} + |1\rangle\langle 1|_a \otimes \mathbb{1} \right) \left( |+\rangle\langle +|_a \otimes U + |-\rangle\langle -|_a \otimes V \right) (|0\rangle_a \otimes |\Psi\rangle) \\
&= \left( |0\rangle\langle 0|_a \otimes \mathbb{1} + |1\rangle\langle 1|_a \otimes \mathbb{1} \right) \left( |+\rangle_a \otimes \langle +|_0\rangle_a U |\Psi\rangle + |-\rangle_a \otimes \langle -|_0\rangle_a V |\Psi\rangle \right) \\
&= |0\rangle_a \otimes \left( \langle 0|+\rangle\langle +|_0\rangle_a U + \langle 0|-\rangle\langle -|_0\rangle_a V \right) |\Psi\rangle + |1\rangle_a \otimes \left( \langle 1|+\rangle\langle +|_0\rangle_a U + \langle 1|-\rangle\langle -|_0\rangle_a V \right) |\Psi\rangle \\
&= |0\rangle_a \otimes \frac{U+V}{2} |\Psi\rangle + |1\rangle_a \otimes \frac{U-V}{2} |\Psi\rangle \\
&\equiv |0\rangle_a \otimes U_+ |\Psi\rangle + |1\rangle_a \otimes U_- |\Psi\rangle.
\end{aligned}$$

Thus, given an initial state of  $|0\rangle_a \otimes |\Psi\rangle$ , the scattered final (normalized) state before the ancilla qubit measurement is

$$|0\rangle_a \otimes U_+ |\Psi\rangle + |1\rangle_a \otimes U_- |\Psi\rangle. \quad (13)$$

During the ancilla qubit measurement, the transition probability  $P_{0 \rightarrow 0}$  ( $P_{0 \rightarrow 1}$ ) for  $|0\rangle_a \rightarrow |0\rangle_a$  ( $|1\rangle_a$ ) is given by squared norms of the interference amplitudes:

$$P_{0 \rightarrow 0} = \|U_+ |\Psi\rangle\|^2 = \left\langle \Psi \left| \frac{(U^\dagger + V^\dagger)(U + V)}{4} \right| \Psi \right\rangle \quad (14)$$

$$= \frac{1}{2} (1 + \text{Re} \langle \Psi | V^\dagger U | \Psi \rangle) \leq 1, \quad (15)$$

$$P_{0 \rightarrow 1} = \|U_- |\Psi\rangle\|^2 = \left\langle \Psi \left| \frac{(U^\dagger - V^\dagger)(U - V)}{4} \right| \Psi \right\rangle \quad (16)$$

$$= \frac{1}{2} (1 - \text{Re} \langle \Psi | V^\dagger U | \Psi \rangle) \leq \frac{1}{4} \|U - V\|^2. \quad (17)$$

Since  $P_{0 \rightarrow 0} + P_{0 \rightarrow 1} = 1$ , we have  $P_{0 \rightarrow 0} \geq \frac{1}{4} - \frac{\|U - V\|^2}{4}$ . Consider the unitary operators  $U = e^{tA}e^{tB}$  and  $V = e^{tB}e^{tA}$ , with  $V^\dagger = V^{-1} = e^{-tA}e^{-tB}$ . Then as  $t \rightarrow 0$ , we have

$$U - V = [A, B]t^2 + \mathcal{O}(t^3), \quad \text{with} \quad (18)$$

$$P_{0 \rightarrow 1} \leq \|U - V\|^2/4 \approx \|[A, B]\|^2 t^4/4, \quad \text{and} \quad (19)$$

$$P_{0 \rightarrow 0} \geq 1 - \|U - V\|^2/4 \approx 1 - \|[A, B]\|^2 t^4/4. \quad (20)$$

Similarly, given an initial state  $|1\rangle_a \otimes |\Psi\rangle$ , the scattered final (normalized) state before the ancilla qubit measurement is

$$|0\rangle_a \otimes U_- |\Psi\rangle + |1\rangle_a \otimes U_+ |\Psi\rangle, \quad (21)$$

and thus we have  $P_{1 \rightarrow 1} = P_{0 \rightarrow 0}$  and  $P_{1 \rightarrow 0} = P_{0 \rightarrow 1}$ .

When the gadget is repeatedly applied, the ancilla measurement outcomes  $(b_1, b_2, \dots, b_\kappa, \dots)$ , with  $b_\kappa \in \{0, 1\}$ , constitute a time-varying Markov chain with the time-dependent transition probability matrix  $\Gamma_\kappa$  (left stochastic matrix convention)

$$\text{Prob}(b_\kappa \rightarrow b_{\kappa+1}) \equiv \Gamma_\kappa = \begin{pmatrix} P_{0_\kappa \rightarrow 0_{\kappa+1}} & P_{1_\kappa \rightarrow 0_{\kappa+1}} \\ P_{0_\kappa \rightarrow 1_{\kappa+1}} & P_{1_\kappa \rightarrow 1_{\kappa+1}} \end{pmatrix}, \quad (22)$$

$$P_{0_\kappa \rightarrow 0_{\kappa+1}} = P_{1_\kappa \rightarrow 1_{\kappa+1}} = \|U_+ |\Psi_\kappa\rangle\|^2, \quad (23)$$

$$P_{0_\kappa \rightarrow 1_{\kappa+1}} = P_{1_\kappa \rightarrow 0_{\kappa+1}} = \|U_- |\Psi_\kappa\rangle\|^2. \quad (24)$$

The  $\Gamma$  is also known as the rate matrix (hence the use of the symbol  $\Gamma$ ). The quantum states  $(|\Psi_1\rangle, |\Psi_2\rangle, \dots, |\Psi_\kappa\rangle, \dots)$  essentially also constitute a Markov chain with state transitions  $|\Psi_{\kappa+1}\rangle = U_\pm |\Psi_\kappa\rangle$  and corresponding transition probabilities  $\|U_\pm |\Psi_\kappa\rangle\|^2$ . Combined with  $(b_1, b_2, \dots, b_\kappa, \dots)$ , our system becomes a hidden quantum Markov model [24].

As a side note, a general LCU of  $U$  and  $V$  can be constructed by replacing the first (second) Hadamard gate

with a general unitary operator  $\hat{G} = \sum_{a,b \in \{0,1\}} g_{ab} |a\rangle\langle b|$  ( $\hat{G}^\dagger$ ). The result is

$$|0\rangle_a \otimes |\Psi\rangle \mapsto |0\rangle_a \otimes [ |g_{00}|^2 U + (1 - |g_{00}|^2) V ] |\Psi\rangle + |1\rangle_a \otimes [ g_{00} g_{01}^* (U - V) ] |\Psi\rangle, \quad (25)$$

$$|1\rangle_a \otimes |\Psi\rangle \mapsto |1\rangle_a \otimes [ |g_{01}|^2 U + (1 - |g_{01}|^2) V ] |\Psi\rangle + |0\rangle_a \otimes [ g_{00}^* g_{01} (U - V) ] |\Psi\rangle, \quad (26)$$

$$P_{0 \rightarrow 1} = P_{1 \rightarrow 0} = 2|g_{00}|^2 |g_{01}|^2 (1 - \text{Re} \langle \Psi | V^\dagger U | \Psi \rangle), \quad (27)$$

$$P_{0 \rightarrow 0} = P_{1 \rightarrow 1} = 1 - P_{0 \rightarrow 1}. \quad (28)$$

In the above, we used the unitary property  $\hat{G}^\dagger \hat{G} = \mathbb{1}$ . Specifically,  $|g_{00}|^2 + |g_{10}|^2 = |g_{01}|^2 + |g_{11}|^2 = 1$  and  $g_{00} g_{01}^* + g_{10} g_{11}^* = g_{01} g_{00}^* + g_{11} g_{10}^* = 0$ . Since  $\hat{G} \hat{G}^\dagger = \mathbb{1}$  is also true, it follows that  $|g_{00}|^2 + |g_{01}|^2 = 1$ . Additionally, we obtain  $P_{0 \rightarrow 1} = P_{1 \rightarrow 0} \leq \frac{1}{2} (|g_{00}|^2 + |g_{01}|^2)^2 (1 - \text{Re} \langle \Psi | V^\dagger U | \Psi \rangle) = \frac{1}{2} (1 - \text{Re} \langle \Psi | V^\dagger U | \Psi \rangle)$  for any  $\hat{G}$ , with the maximal value achieved whenever  $|g_{00}| = |g_{01}| = |g_{10}| = |g_{11}| = 1/\sqrt{2}$ . In particular, the Hadamard gate case corresponds to  $(g_{00}, g_{01}, g_{10}, g_{11}) = (1, 1, 1, -1)/\sqrt{2}$  with a maximal  $P_{0 \rightarrow 1} = P_{1 \rightarrow 0}$  (and hence a minimal  $P_{0 \rightarrow 0} = P_{1 \rightarrow 1}$ ) for any fixed  $U, V$ , and  $|\Psi\rangle$ .

### III. APPLICATIONS

#### A. TRIS (Breaking) Spectral Walk

In addition to the quantum simulation of complex objects, quantum computers offer an avenue to probe fundamental concepts such as the emergence or breaking of a symmetry [25]. Time-reversal is one such symmetry whose presence has fundamental consequences for the resulting spectra (Kramers' Theorem) and dynamics. An operator is time-reversal inversion symmetric (TRIS) if it is invariant under  $t \rightarrow -t$ .

We use this fact and the Jordan-product to define an algorithm for TRIS (breaking) quantum random walks. Motivated by near-term resource limitations, we focus on the stabilization of a TRIS random walk. Then we discuss the extent to which random coherent imprecision can break the time reversal symmetry. Steps to recover TRIS are discussed as well.

##### 1. Analysis of a single step

Consider the Jordan forms as the linear operators comprised of forward and backwards time evolutions:

$$U_+(t) = \frac{U(t) + U(-t)}{2} = \frac{e^{-iHt} + e^{iHt}}{2} = +\cos(Ht),$$

$$U_-(t) = \frac{U(t) - U(-t)}{2} = \frac{e^{-iHt} - e^{iHt}}{2} = -i\sin(Ht).$$

In this special example, where  $V = [U(t)]^\dagger = U(-t)$ , the time-reversed evolutions interfere such that the overlap factors becomes  $\text{Re} \langle \Psi | V^\dagger U | \Psi \rangle = \text{Re} \langle \Psi | U^2 | \Psi \rangle = \langle \Psi | \cos 2Ht | \Psi \rangle \equiv \cos 2Et$  (for small  $|t|$  and  $E \approx \langle \Psi | H^2 | \Psi \rangle^{1/2}$ ). The ancilla transition probabilities then encode the trigonometric power reduction relations, namely  $P_{0 \rightarrow 0} = (1 + \cos 2Et)/2 = \cos^2 Et$  and similarly,  $P_{0 \rightarrow 1} = (1 - \cos 2Et)/2 = \sin^2 Et$ .

##### 2. Spectral projection by random walks

The principal system evolves the normalized state  $|\Phi\rangle = \cos(Ht)|\Psi\rangle/\sqrt{P_{0 \rightarrow 0}} - i\sin(Ht)|\Psi\rangle/\sqrt{P_{0 \rightarrow 1}}$  with probability  $P_{0 \rightarrow 0}$  ( $P_{0 \rightarrow 1}$ ). For a single step walk, the mixed state density operator, which begins as a pure initial state  $\rho(0) \equiv \rho \equiv |\Psi\rangle\langle\Psi|$ , is

$$\rho(t) = \cos(Ht)\rho\cos(Ht) + \sin(Ht)\rho\sin(Ht) \quad (29)$$

$$\equiv \mathcal{K}_{0,t}(\rho) + \mathcal{K}_{1,t}(\rho) = \mathcal{H}_t^{\text{cs}}(\rho) \quad (30)$$

is used to describe the measurements of an observable  $\hat{O}$  on the principal system with many shots. The evolution above is non-unitary, but rather described by a Lindblad evolution process, as a sum of Kraus maps  $\mathcal{K}_{0,t}(\rho) = \cos(Ht)\rho\cos(Ht)$  and  $\mathcal{K}_{1,t}(\rho) = \sin(Ht)\rho\sin(Ht)$ . Since the density operator under unitary evolution channel is

$$\rho_U(t) = \mathcal{H}_t(\rho) = e^{-iHt}\rho e^{iHt} \quad (31)$$

$$= \cos(Ht)\rho\cos(Ht) + \sin(Ht)\rho\sin(Ht) + i\cos(Ht)\rho\sin(Ht) - i\sin(Ht)\rho\cos(Ht), \quad (32)$$

we have  $\rho(t) = [\rho_U(t) + \rho_U(-t)]/2$ . To prove that eigenstates are fixed points of the spectral walk dynamics, we refer to the proof of Ref. 26, where we use  $p_1 = 1/2 = p_2$  and  $U_1 = U(t), U_2 = U_1^\dagger = U(-t)$ . This means that our time evolution channel given by Eq. (29) is TRIS if we do not post-select the ancilla measurement outcome strings. In addition, it conserves the energy  $\text{Tr}(\rho(t)H) = \text{Tr}(\rho(0)H) = \langle \Psi | H | \Psi \rangle$ .

In the energy eigenbasis of the Hermitian Hamiltonian,  $\{(\omega_n, |n\rangle)\}$ , where  $H|n\rangle = \omega_n|n\rangle$  with  $\omega_n \in \mathbb{R}$ , the initial pure state is  $|\Psi\rangle = \sum_n c_n |n\rangle$ . The density matrix is then  $\rho = \sum_{n,m} c_n c_m^* |n\rangle\langle m| = \sum_k |c_k|^2 |k\rangle\langle k| + \sum_{n \neq m} c_n c_m^* |n\rangle\langle m| \equiv \rho^{\text{d}} + \rho^{\text{od}}$ , where  $\rho^{\text{d}}$  ( $\rho^{\text{od}}$ ) is the diagonal (off-diagonal) part of the density operator in the energy eigenbasis. We can assume that there is no degeneracy in  $\rho^{\text{od}}$  part, i.e.,  $\omega_n \neq \omega_m$  for  $n \neq m$ <sup>2</sup>. The

<sup>2</sup> Should there be any degeneracy, a unitary transformation within the degenerate subspace can put those terms into the  $\rho^{\text{d}}$  part, while all new basis states are still energy eigenstates. In the case of pure-state density operator  $|\Psi\rangle\langle\Psi|$  with  $|\Psi\rangle = \sum_n c_n |n\rangle$ , this transformation can be simply done by grouping all degenerate eigenstates corresponding to the same eigenenergy into a new eigenstate with a proper normalization.

operator  $\rho^d$  does not evolve with time since  $\mathcal{H}_t^{\text{cs}}(\rho^d) = \mathcal{H}_t(\rho^d) = \rho^d$ . In other words,  $\rho^d$  is a fixed point for both  $\mathcal{H}_t^{\text{cs}}$  and  $\mathcal{H}_t$ , however the corresponding stability of this fixed point is different. To see this, for a short time  $|t|$ , comparing

$$\begin{aligned}\rho_U(t) &= \rho - it[H, \rho] - \frac{t^2}{2}[H, [H, \rho]] + \mathcal{O}(t^3) \\ &= \rho^d + \rho^{\text{od}} - it[H, \rho^{\text{od}}] - \frac{t^2}{2}[H, [H, \rho^{\text{od}}]] + \mathcal{O}(t^3),\end{aligned}$$

with

$$\begin{aligned}\rho(t) &= \frac{\rho_U(t) + \rho_U(-t)}{2} = \rho - \frac{t^2}{2}[H, [H, \rho]] + \mathcal{O}(t^4) \\ &= \rho^d + \rho^{\text{od}} - \frac{t^2}{2}[H, [H, \rho^{\text{od}}]] + \mathcal{O}(t^4),\end{aligned}$$

and using

$$\begin{aligned}\rho^{\text{od}} - it[H, \rho^{\text{od}}] &= \sum_{n \neq m} [1 - it(\omega_n - \omega_m)] c_n c_m^* |n\rangle\langle m|, \quad (33)\end{aligned}$$

$$\begin{aligned}\rho^{\text{od}} - \frac{t^2}{2}[H, [H, \rho^{\text{od}}]] &= \sum_{n \neq m} \left[ 1 - \frac{t^2(\omega_n - \omega_m)^2}{2} \right] c_n c_m^* |n\rangle\langle m|, \quad (34)\end{aligned}$$

we find that the off-diagonal part of time-evolved density operator  $\rho(t)$  contracting but not the off-diagonal part of  $\rho_U(t)$  due to the first order term. Therefore, if we apply the channel  $\mathcal{H}_t^{\text{cs}}$  iteratively as  $\prod_{\kappa=1}^r \mathcal{H}_{t_\kappa}^{\text{cs}} = \prod_{\kappa=1}^r (\mathcal{K}_{0, t_\kappa} + \mathcal{K}_{1, t_\kappa})$ , then the final density matrix will contract to the fixed point  $\rho^d = \sum_k |c_k|^2 |k\rangle\langle k|$  without any remaining interference terms from  $\rho^{\text{od}}$ .

For a multi-step random walk, discussed below in Sec. III A 3, with a definitive path indicated by the ancilla measurement outcome  $r$ -bit string, such as  $\mathbf{b} = (b_1, b_2, \dots, b_r) = (0, 1, \dots, 1)$ , a single term  $\prod_{\kappa=1}^r \mathcal{K}_{b_\kappa, t_\kappa} \equiv \mathcal{K}_{\mathbf{b}, \mathbf{t}}$  from the series product should be applied instead. The specific form for  $\mathcal{K}_{\mathbf{b}, \mathbf{t}}$  is  $\mathcal{K}_{\mathbf{b}, \mathbf{t}}(\rho) = (K_{b_r, t_r} \cdots K_{b_1, t_1}) \rho (K_{b_1, t_1}^\dagger \cdots K_{b_r, t_r}^\dagger) \equiv K_{\mathbf{b}, \mathbf{t}}(\rho) K_{\mathbf{b}, \mathbf{t}}^\dagger$ , where  $K_{0, t} = \cos(Ht)$  and  $K_{1, t} = \sin(Ht)$ . This results in a pure-state density matrix  $\rho_{\mathbf{b}, \mathbf{t}} = K_{\mathbf{b}, \mathbf{t}}(|\Psi\rangle\langle\Psi|) K_{\mathbf{b}, \mathbf{t}}^\dagger / P(\mathbf{b}, \mathbf{t})$ , where  $P(\mathbf{b}, \mathbf{t}) = \langle\Psi|K_{\mathbf{b}, \mathbf{t}}^\dagger K_{\mathbf{b}, \mathbf{t}}|\Psi\rangle$ .

For sufficiently large  $r$  and  $\mathbf{b} \in B \subset \{0, 1\}^r$ , we have  $\rho_{\mathbf{b}}^d = |k_{\mathbf{b}}\rangle\langle k_{\mathbf{b}}|$ , where  $|k_{\mathbf{b}}\rangle$  is one of the energy eigenstates projected out after the random walk along the path  $\mathbf{b}$  (from now on, we suppress the  $\mathbf{t}$  dependence). Numerical experiments seem to indicate  $|B| \sim |\{0, 1\}^r| = 2^r$ , i.e.,  $\sum_{\mathbf{b} \in B} P(\mathbf{b}) \sim 1$ . Since the sum of all  $2^r$  paths recovers  $\sum_{\mathbf{b}} P(\mathbf{b}) \rho_{\mathbf{b}} = \sum_{\mathbf{b}} \mathcal{K}_{\mathbf{b}}(|\Psi\rangle\langle\Psi|) = \rho^d = \sum_k |c_k|^2 |k\rangle\langle k|$  and  $\sum_{\mathbf{b}} P(\mathbf{b}) \rho_{\mathbf{b}} \sim \sum_{\mathbf{b} \in B} P(\mathbf{b}) |k_{\mathbf{b}}\rangle\langle k_{\mathbf{b}}| =$

$\sum_k (\sum_{\mathbf{b} \in B_k} P(\mathbf{b})) |k\rangle\langle k|$ , where  $\bigcup_k B_k = B$ , we conclude that there should be  $\approx |B| |c_k|^2$  paths that project out the energy eigenstate  $|k\rangle$ , or equivalently, the probability  $P(|k\rangle | \mathbf{b} \in B) = \sum_{\mathbf{b} \in B_k} P(\mathbf{b}) = |c_k|^2$ .

To efficiently project out the eigenenergy spectrum, we need to choose proper time step sizes  $\{t_\kappa\}_{\kappa=1}^r$ . First, for very short time evolution step sizes,  $P_{0 \rightarrow 0} \gg P_{0 \rightarrow 1}$ . In this case, consecutive  $\cos(Ht)$  operators are applied to the state with high probability and the resulting operator  $\cos^r(Ht) = e^{r \log[\cos(Ht)]} \approx e^{-rH^2 t^2/2}$  projects out the ground state (assume the spectrum is shifted to  $\geq 0$  and there is finite overlap between the ground state and initial state [27–29]). Therefore, we can apply this algorithm to prepare ground state by frequently measuring the ancilla. However, too frequent measurements would result in non-evolving initial state due to quantum Zeno effect (QZE). If this happens, we would have a quadratically stronger QZE (i.e., slower evolution) due to the time evolution operator  $\cos(Ht)$  instead of the usual  $e^{-iHt}$ . We check this in Appendix A by computing  $\lim_{n \rightarrow \infty} S_n(T/n)$ , conditioned that the ancilla measurement is always 0, where the survival probability  $S_n(T/n) = |\langle\Psi|\Phi\rangle|^2$  and the time evolved final state is  $|\Phi\rangle = \cos^n(HT/n) |\Psi\rangle / [\langle\Psi|\cos^{2n}(HT/n)|\Psi\rangle]^{1/2}$ . A subtle difference with a textbook QZE is that the principal system can be kept stationary by measuring an ancillary system that couples to the principal system. In a textbook example, the principal system is directly measured. This provides an advantage to use our setting to observe or achieve the QZE since measuring a single ancilla qubit is much simpler than measuring the entire principal system.

To find a suitable time step sizes for spectral projection, we rewrite Eq. (29) in the energy eigenbasis:

$$\begin{aligned}\rho(t) &= \rho^d + \sum_{n \neq m} [\cos(\omega_n t) \cos(\omega_m t) \\ &\quad + \sin(\omega_n t) \sin(\omega_m t)] c_n c_m^* |n\rangle\langle m| \\ &= \rho^d + \sum_{n \neq m} \cos[(\omega_n - \omega_m)t] c_n c_m^* |n\rangle\langle m|. \quad (35)\end{aligned}$$

After  $r$  steps, the coefficient for  $|n\rangle\langle m|$  is suppressed by a factor  $\prod_{\kappa=1}^r \cos[(\omega_n - \omega_m)t_\kappa]$ . Since  $|\cos[(\omega_n - \omega_m)t_\kappa]| \leq 1$  and  $\omega_n \neq \omega_m$  for  $n \neq m$ , the projection will always success for sufficiently large  $r$  and any set of  $t_\kappa$ 's  $\not\equiv 0 \pmod{\pi/|\omega_n - \omega_m|}$  larger than the QZE time scale set by  $1/r$ .

### 3. Analysis of semi-coherent multi-step random walk

In Sec. III A 2, both the ancilla qubit and the principal system evolve incoherently and stochastically step by step. After passing the *mixing time* [30], the principal system converges to a *stationary* mixed state  $\rho = \sum_k |c_k|^2 |k\rangle\langle k|$  that is diagonal in the energy eigenbasis. The population of the energy eigenstates are given by

the Born's rule probabilities, which is determined by the initial pure state  $|\Psi\rangle = \sum_k c_k |k\rangle$ . Here, we consider multi-step random walk (assume  $r$  total steps) with semi-coherent evolutions. i.e., after  $r$  steps, the quantum state principal system remains pure.

We start from an initial state  $|\Psi_0\rangle$ . At each clock-cycle  $\kappa \in \{1, 2, \dots, r\}$ , select a random variable  $t_\kappa$ . Using an ancilla qubit and evolve according to the evolution  $\frac{1}{2}[e^{-iHt_\kappa} + (-1)^{b_\kappa} e^{iHt_\kappa}]$ , where  $b_\kappa = m_{\kappa-1} \oplus m_\kappa$  without resetting the ancilla,  $b_\kappa = 0 \oplus m_\kappa$  with resetting the ancilla to  $|0\rangle_a$ , and  $m_\kappa \in \{0, 1\}$  is the measurement outcome obtained at the end of this cycle  $\kappa$ . After  $r$  clock-cycles the state has evolved from  $|\Psi_0\rangle$  to  $|\Psi_r\rangle = F_r |\Psi_0\rangle$  (not normalized) according to  $F_r = \prod_{\kappa=1}^r f_{a_\kappa}(Ht_\kappa)$ , where  $f_{a_\kappa=0}(\cdot) = \cos(\cdot)$ , occurring with probability as above  $P_{0 \rightarrow 0} = \cos^2 E_{r-1} t_r$ . Similarly,  $f_{a_\kappa=1}(\cdot) = -i \sin(\cdot)$  with probability  $P_{0 \rightarrow 1} = \sin^2 E_{r-1} t_r$ , where  $\cos 2E_{r-1} t_r = \langle \Psi_{r-1} | \cos 2Ht_r | \Psi_{r-1} \rangle / \langle \Psi_{r-1} | \Psi_{r-1} \rangle = \langle \Psi_0 | (\cos 2Ht_r) F_{r-1}^\dagger F_{r-1} | \Psi_0 \rangle / \langle \Psi_0 | F_{r-1}^\dagger F_{r-1} | \Psi_0 \rangle$  (note that  $[H, F_r] = 0$ ).

Since the relative ratio of  $P_{0 \rightarrow 0} / P_{0 \rightarrow 1} = \cot^2 Et$ , it follows that the ancilla qubit realizes a heavily-biased random coin producing many strings of  $a_\kappa = 0$  interspersed with the odd counter driving term  $-i \sin Ht$ . TRIS-preserving operator strings reduce to  $\cos_Q^\kappa(Ht)$ , which can be expanded into a binomial expansion using the trig identity  $\cos^2 Ht = (\mathbb{1} + \cos(2Ht))/2$ . Again, using our prior trick,  $\sin^2 Ht = (\mathbb{1} - \cos(2Ht))/2$ , the *product* of two TRIS-breaking terms *preserves* the TRIS. While actions at different times have opposite temporal parities, they nevertheless commute so that  $\prod_{\kappa=1}^r f_{a_\kappa}(Ht_\kappa) = \prod_{\kappa \in \mathcal{I}_0} \cos(Ht_\kappa) \times (-i)^{|\mathcal{I}_1|} \prod_{\kappa \in \mathcal{I}_1} \sin(Ht_\kappa)$ , where  $\mathcal{I}_0 = \{\kappa \in [r] \mid a_\kappa = 0\}$ , and  $\mathcal{I}_1 = \{\kappa \in [r] \mid a_\kappa = 1\}$ . That is, any configuration with an *even* number (denoted as  $|\mathcal{I}_1|$ ) of  $0 \rightarrow 1$  outcomes is a valid TRIS coherent configuration, while those with  $|\mathcal{I}_1|$  *odd* break the TRIS. It's easy to see that breaking TRIS and breaking the Hermiticity of the  $F_r$  operator occur in tandem.

Additionally, the times  $t_\kappa$  can be adjusted to explore different TRIS distributions. The general expres-

sion can likewise be factorized using  $\cos Ht \cos H\tau = (\cos(H(t-\tau)) + \cos(H(t+\tau)))/2$ . In the construction above, we constructed an operator  $\propto U(t) + U(-t)$ . Let us generically consider a case where a control error  $2\delta$  is present in the form:

$$\begin{aligned} U(t) + U(-t + 2\delta) &= (U(t - \delta) + U(-t + \delta))U(\delta) \\ &= \cos(t - \delta) (\cos(\delta) + i \sin(\delta)). \end{aligned}$$

As the backwards time-evolution was shortened by a factor  $2\delta$ , we interpret the expression above as a transformation to a center-of-time coordinate, namely  $t_c = t - \delta$  and a relative-time coordinate  $\delta$ . The first term, which is a product of cosines, is time-reversal symmetric while the second term, involving the sine, breaks the TRIS.

### B. Trotter Factorized Spin Procession

The simplest model is a single qubit system, as both its true dynamics and the approximate Trotter dynamics [31] can be exactly solved on the Bloch sphere. A general one-qubit Hamiltonian is described as

$$H_{1q} = \sum_{\alpha=0}^3 d_\alpha \hat{\sigma}^\alpha, \quad (36)$$

where  $d_\alpha \in \mathbb{R}$  for a Hermitian Hamiltonian, and the Pauli matrices are denoted by  $\hat{\sigma}^0 = \mathbb{1} = \begin{pmatrix} 1 & 0 \\ 0 & 1 \end{pmatrix}$ ,  $\hat{\sigma}^1 = X = \begin{pmatrix} 0 & 1 \\ 1 & 0 \end{pmatrix}$ ,  $\hat{\sigma}^2 = Y = \begin{pmatrix} 0 & -i \\ i & 0 \end{pmatrix}$ , and  $\hat{\sigma}^3 = Z = \begin{pmatrix} 1 & 0 \\ 0 & -1 \end{pmatrix}$ . For simplicity, consider  $d_0 = d_3 = 0$  and denote the complex number  $d_1 + id_2 = de^{i\theta} = d \cos \theta + id \sin \theta$ , where  $d = \sqrt{d_1^2 + d_2^2}$  and  $\theta = \text{Arg}(d_1 + id_2) \in (-\pi, \pi]$ . Then,

$$H_{1q} = d_1 X + d_2 Y = d(\cos \theta X + \sin \theta Y). \quad (37)$$

The exact dynamics is given by

$$U(t) = e^{-itH_{1q}} \quad (38)$$

$$= \cos(td) \mathbb{1} - i \sin(td) (\cos \theta X + \sin \theta Y). \quad (39)$$

The second order linear combination of Trotter unitaries (LCTU) is

$$2U_+(t) = e^{-itd_1 X} e^{-itd_2 Y} + e^{-itd_2 Y} e^{-itd_1 X} \quad (40)$$

$$= 2 \cos(td_1) \cos(td_2) \mathbb{1} - 2i \cos(td_2) \sin(td_1) X - 2i \cos(td_1) \sin(td_2) Y \quad (41)$$

$$= \cos(t(d_1 + d_2)) \mathbb{1} - i(X + Y) \sin(t(d_1 + d_2)) + \cos(t(d_1 - d_2)) \mathbb{1} - i(X - Y) \sin(t(d_1 - d_2)) \quad (42)$$

$$= U(t(d_1 + d_2)) + \tilde{U}(t(d_1 - d_2)), \quad (43)$$

where  $\tilde{U}$  is the additive error due to phase, which is generated by  $\cos(\theta)X + \sin(\theta + \pi)Y$  and vanishes if  $d_1 = d_2$ . To characterize the approximation error, we compute the Frobenius norm<sup>3</sup>  $\|U_+(t) - U(t)\|$ .

$$\|U_+(t) - U(t)\|$$

<sup>3</sup> The Frobenius norm is defined as  $\|A\|_F = [\text{Tr}(A^\dagger A)]^{1/2}$ . Note that the operator norm is an upper bound of the Trotter error for state time evolution  $\|\delta U |\Psi\rangle\| \leq \|\delta U\| \|\Psi\| = \|\delta U\|$ , assuming  $|\Psi\rangle$  is normalized.

$$= \|\cos(td_1)\cos(td_2) - \cos(td)\mathbb{1} - i[\cos(td_2)\sin(td_1) - \sin(td)\cos\theta]X - i[\cos(td_1)\sin(td_2) - \sin(td)\sin\theta]Y\| \quad (44)$$

$$= \sqrt{2}\{[\cos(td_1)\cos(td_2) - \cos(td)]^2 + [\cos(td_2)\sin(td_1) - \sin(td)\cos\theta]^2 + [\cos(td_1)\sin(td_2) - \sin(td)\sin\theta]^2\}^{1/2} \quad (45)$$

$$= \begin{cases} 0, & \theta \in \{0, \pi, \pm\frac{\pi}{2}\} \\ \frac{\sqrt{2}}{6} |(td)^3 \sin(2\theta)| + \mathcal{O}(t^5), & \theta \notin \{0, \pi, \pm\frac{\pi}{2}\}. \end{cases} \quad (46)$$

In the above, we used the identity (for  $c_\alpha \in \mathbb{R}$ )

$$\left\| c_0 \hat{\sigma}^0 \pm i \sum_a c_a \hat{\sigma}^a \right\| = \left\{ \text{Tr} \left[ \left( c_0 \hat{\sigma}^0 + i \sum_a c_a \hat{\sigma}^a \right) \left( c_0 \hat{\sigma}^0 - i \sum_a c_a \hat{\sigma}^a \right) \right] \right\}^{1/2} = \sqrt{2} \left( \sum_{\alpha=0}^3 c_\alpha^2 \right)^{1/2}.$$

On the other hand, the conventional second order Trotter  $U_{(2)}(t)$  is given by

$$U_{(2)}(t) = e^{-itd_1 X/2} e^{-itd_2 Y} e^{-itd_1 X/2} \quad (47)$$

$$= \cos(td_1)\cos(td_2)\mathbb{1} - i\cos(td_2)\sin(td_1)X - i\sin(td_2)Y. \quad (48)$$

Comparing to the SU(2) formula for the exponential of a Pauli vector,  $e^{-i\phi\hat{\mathbf{n}}\cdot\boldsymbol{\sigma}} = \mathbb{1}\cos\phi - i(\hat{\mathbf{n}}\cdot\boldsymbol{\sigma})\sin\phi$ , we have

$$z_{(2)} = \log(U_{(2)}) = -i\phi_{(2)}(n_{(2)}^x X + n_{(2)}^y Y), \quad (49)$$

$$\cos\phi_{(2)} = \cos(td_1)\cos(td_2), \quad (50)$$

$$n_{(2)}^x = \cos(td_2)\sin(td_1)/\sin\phi_{(2)}, \quad (51)$$

$$n_{(2)}^y = \sin(td_2)/\sin\phi_{(2)}. \quad (52)$$

It's easy to verify that  $(n_{(2)}^x)^2 + (n_{(2)}^y)^2 = 1$ , so  $U_{(2)}(t)$  is indeed a unitary operator. In general,  $U_+(t)$  is not a unitary operator. However, we can define  $U_+ = e^{-\alpha}U'_+$ , where  $U'_+ = e^\alpha U_+$  is unitary and

$$z_+ = \log(e^{-\alpha}U'_+) = -i\phi_+(n_+^x X + n_+^y Y) - \alpha\mathbb{1}, \quad (53)$$

$$\alpha = -\frac{1}{2} \log [1 - \sin^2(td_1)\sin^2(td_2)] > 0, \quad (54)$$

$$\cos\phi_+ = e^\alpha \cos(td_1)\cos(td_2) \in (-1, 1), \quad (55)$$

$$n_+^x = e^\alpha \cos(td_2)\sin(td_1)/\sin\phi_+, \quad (56)$$

$$n_+^y = e^\alpha \cos(td_1)\sin(td_2)/\sin\phi_+. \quad (57)$$

We can verify  $(n_+^x)^2 + (n_+^y)^2 = 1$  so  $U'_+(t)$  is a unitary. Note that if  $\sin^2(td_1)\sin^2(td_2) = 1$ , then  $\alpha = \infty$  and  $U_+ = 0$ , which indicates large Trotter error. However, this won't happen if  $|td_1|, |td_2| \ll 1$ . The success probability is  $P_{0 \rightarrow 0} = \|U_+|\Psi\rangle\|^2 = \langle\Psi|U_+^\dagger U_+|\Psi\rangle = e^{-2\alpha} = 1 - \sin^2(td_1)\sin^2(td_2) = 1 - d_1^2 d_2^2 t^4 + \mathcal{O}(t^6)$ , which is independent of the state vector  $|\Psi\rangle$ . Eq. (20) gives  $P_{0 \rightarrow 0} \geq 1 - d_1^2 d_2^2 t^4 / 2$  (because  $\|[A, B]\|^2 = d_1^2 d_2^2 \|Z\|^2 = 2d_1^2 d_2^2$ ). If successful, the normalized state after measurement of ancilla is  $|\Psi(t)\rangle = U_+(t)|\Psi\rangle / \sqrt{P_{0 \rightarrow 0}} = U'_+(t)|\Psi\rangle$ , so  $U'_+(t)$  is the effective unitary of the LCTU algorithm.

Finally, the norm distance between  $U_+$  and the unitary  $U'_+$  is  $\|U_+(t) - U'_+(t)\| = \frac{\sqrt{2}}{8}(td)^4 \sin^2(2\theta)$ , which is not to the same order of the squared Trotter error  $\|U_+(t) - U(t)\|$  as it would be for the multi-product formulas (see the top of Page 5 of Ref. 1).

The error of the second order Trotter is given by the operator norm

$$\|U_{(2)}(t) - U(t)\| = \|\cos(td_1)\cos(td_2) - \cos(td)\mathbb{1} - i[\cos(td_2)\sin(td_1) - \sin(td)\cos\theta]X - i[\sin(td_2) - \sin(td)\sin\theta]Y\| \quad (58)$$

$$= \sqrt{2}\{[\cos(td_1)\cos(td_2) - \cos(td)]^2 + [\cos(td_2)\sin(td_1) - \sin(td)\cos\theta]^2 + [\sin(td_2) - \sin(td)\sin\theta]^2\}^{1/2} \quad (59)$$

$$= \begin{cases} 0, & \theta \in \{0, \pi, \pm\frac{\pi}{2}\}; \\ \frac{\sqrt{5-3\cos(2\theta)}}{12} |(td)^3 \sin(2\theta)| + \mathcal{O}(t^5), & \theta \notin \{0, \pi, \pm\frac{\pi}{2}\}. \end{cases} \quad (60)$$

The errors are plotted in Fig. 2. Since  $\sqrt{2}/12 = \sqrt{5-3}/12 \leq \sqrt{5-3\cos(2\theta)}/12 \leq \sqrt{5+3}/12 = \sqrt{2}/6$ , it follows



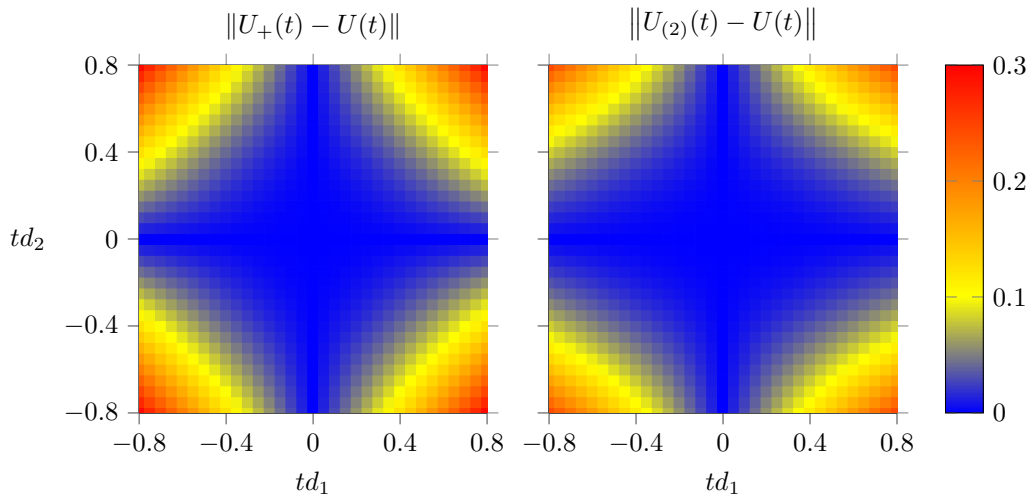


FIG. 2. Comparison of the operator norm error between two-unitary LCTU  $U_+(t)$  and the second order Trotter  $U_{(2)}(t)$  in approximating the exact unitary  $U(t)$ . Generally,  $U_{(2)}$  has smaller error than  $U_+$ . The error plot's symmetry can be understood from their respective small  $t$  expansion:  $U_+(t)$  has four-fold symmetry due to  $|\sin(2\theta)|$  factor, while  $U_{(2)}(t)$  only has two-fold symmetry due to additional  $\sqrt{5 - 3\cos(2\theta)}$  factor.

that the error of second order Trotter is always smaller than the two-unitary LCTU for this model. However, if  $\theta = \frac{\pi}{4}$ , the  $X \leftrightarrow Y$  symmetry of the  $H_{1q}$  conserved by the  $U_+(t)$  evolution can have certain advantage over  $U_{(2)}$  that breaks this symmetry. For instance, when acted on the eigenstates of  $H_{1q}$ , the second order LCTU  $U_+(t)$  gives a correct dynamic phase with  $t^3$  error and keeps the eigenstates stationary on Bloch sphere as the exact evolution  $U(t)$  does, but  $U_{(2)}(t)$  will rotate these states on Bloch sphere.

### C. Symmetrized Hamiltonian Variational Ansatz for the Heisenberg Chain

Solving the ground state (GS) and the ground state energy (GSE) of Hamiltonians of general quantum systems is a challenging problem and typically Quantum-Merlin-Arthur (QMA) hard [32, 33], which is quantum analogous to NP hard in classical computing. The variational quantum eigensolver (VQE) is the most practical quantum-classical hybrid algorithm to tackle this problem on NISQ quantum hardware. Among a plethora of ansatzes implementing VQEs, the Hamiltonian variational ansatz (HVA) stands out as a physics informed approach. It utilizes a single unitary product composed of factors derived from a one-step Trotter formula, enabling the time-evolution unitary of a Hamiltonian. The HVA has demonstrated significant strength in solving the GS problems from chemistry and physics [34] as it encodes adiabatic evolutions for these general systems as the quantum approximate optimization algorithm (QAOA) does for the Ising spin models.

To improve algorithmic efficiency, and reduce both quantum and classical computing resources, symmetry-preserving (-adapted) VQEs have been recently proposed[35]. However, existing implementations often incur large circuit depth and gate budget overhead for symmetry preservation or projection. Inspired by the commutative symmetry of Jordan algebras, we propose a

symmetrized HVA, termed symHVA using LCTU products. Applying symHVA to the 8-site Heisenberg spin chain, we find significantly improved performance compared to HVA.

First, we define the Heisenberg model before showing the symHVA result compared with conventional HVA. The general spin- $\frac{1}{2}$  Heisenberg XYZ model [without local Zeeman ( $\hbar^z S_l^z$  terms) or transverse ( $\hbar^x S_l^x$  and  $\hbar^y S_l^y$  terms) fields] on an  $L$ -site chain is defined as

$$H_{XYZ} = \sum_{l=0}^{L-1} (J_x S_l^x S_{l+1}^x + J_y S_l^y S_{l+1}^y + J_z S_l^z S_{l+1}^z), \quad (61)$$

where  $S_l^a = \frac{\hbar}{2}\sigma_l^a$ , for  $a \in \{x, y, z\}$ . The periodic boundary condition (i.e., a circular chain) is considered in Eq. (61), so  $l + 1 \equiv 0 \pmod{L}$  for  $l = L - 1$  in the sum (for open boundary condition, the sum upper limit is  $l = L - 2$ ). From now on, we consider the special case with isotropic antiferromagnetic interactions  $J_x = J_y = J_z \equiv J > 0$  (i.e., the XXX Heisenberg model) and choose the units of energy so that  $\frac{J\hbar}{4} = 1$ . Then, the simplified antiferromagnetic Heisenberg model (AFHM) is

$$H = \sum_{l=0}^{L-1} (X_l X_{l+1} + Y_l Y_{l+1} + Z_l Z_{l+1}) \quad (62)$$

$$\equiv \sum_{l=0}^{L-1} H_l = \sum_{l=0}^{L-1} \boldsymbol{\sigma}_l \cdot \boldsymbol{\sigma}_{l+1} \quad (63)$$

$$= \sum_{\text{even } l} \boldsymbol{\sigma}_l \cdot \boldsymbol{\sigma}_{l+1} + \sum_{\text{odd } l} \boldsymbol{\sigma}_l \cdot \boldsymbol{\sigma}_{l+1} \equiv H_A + H_B. \quad (64)$$

In the above,  $\boldsymbol{\sigma}_l \equiv (X_l, Y_l, Z_l)$ . For an even number of sites  $L$ , the chain is a bipartite lattice, and the  $A$  ( $B$ ) part defined in Eq. (64) is referred as the  $A$  ( $B$ ) sublattice.

We solve our AFHM ground state problem by

$$\min_{\boldsymbol{\theta}} \frac{\langle \psi_0 | U^\dagger(\boldsymbol{\theta}) \hat{H} U(\boldsymbol{\theta}) | \psi_0 \rangle}{\langle \psi_0 | U^\dagger(\boldsymbol{\theta}) U(\boldsymbol{\theta}) | \psi_0 \rangle}. \quad (65)$$

We choose a good initial trial state  $|\psi_0\rangle = \frac{\sqrt{2}}{3}(|\psi_{0A}\rangle + |\psi_{0B}\rangle)$ , where  $|\psi_{0A}\rangle$  ( $|\psi_{0B}\rangle$ ) is a valence bond state with singlet bonds on blue (red) edges as shown by an 8-vertex cycle graph inset in Fig. 3. (The  $\frac{\sqrt{2}}{3}$  normalization factor is due to that the two valence bond states  $|\psi_{0A}\rangle$  and  $|\psi_{0B}\rangle$  are not orthogonal.)  $U(\boldsymbol{\theta})$  is unitary in HVA, with each circuit layer given by  $e^{i \sum_l \theta_l^p H_l}$  (total  $8p$  parameters for  $p$  layers); in symHVA,  $U(\boldsymbol{\theta})$  is nonunitary with each layer given by

$$U_{A,B}(\theta_1^p, \theta_2^p) = \frac{1}{2} \left( e^{i\theta_1^p H_A} e^{i\theta_2^p H_B} + e^{i\theta_1^p H_B} e^{i\theta_2^p H_A} \right) \quad (66)$$

with total  $2p$  parameters.  $p = 2$  is sufficient for symHVA to reach the exact ground state energy (GSE) within (classical) machine precision, as shown in Fig. 3.

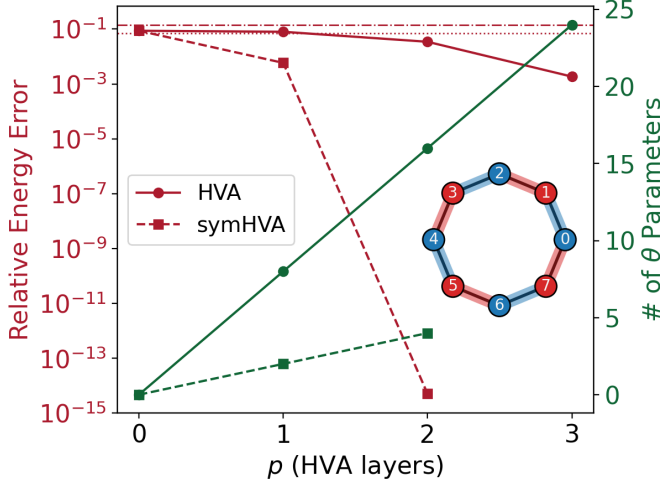


FIG. 3. Red lines, left axis: relative error between optimized GSE and the exact one as a function of the number of HVA layers. Green lines, right axis: total number of variational parameters used in HVA and symHVA. Inset: graph representation of the 8-site AFHM. Two red horizontal lines are two reference energies relative to the GSE: the first excited energy (dash-dotted line) and the energy at the middle point of the gap (dotted line).

#### D. Mermin Polynomial Measure for Multi-Partite Entanglement

Above, we saw how symmetries can impact dynamical processes in three settings. We turn our attention to quantum processes measurement. This subsection culminates by demonstrating a duality between destructive and non-destructive ancilla-mediated measurements.

Mermin polynomials appear in the Mermin-Klyshko (MK) inequalities [36] that are a multi-partite generalization of the two-particle Clauser-Horne-Shimony-Holt (CHSH) inequality. Mermin [36, Eq. (3)] proposed the degree- $n$  homogeneous polynomial that is a sum of degree- $n$  monomials  $\pm \prod_{l=1}^n (\sigma_l^x)^{p_l^x} (\sigma_l^y)^{p_l^y}$  in terms of  $n$  pairs of spin operators  $\{(\sigma_l^x, \sigma_l^y) \mid l = 1, 2, \dots, n\}$  and binary symplectic vectors in the subspace  $\{(\mathbf{p}^x, \mathbf{p}^y) \mid \mathbf{p}^x = (p_1^x, \dots, p_n^x), \mathbf{p}^y = (p_1^y, \dots, p_n^y), p_l^x, p_l^y \in \mathbb{Z}_2, p_l^x + p_l^y \equiv 1 \pmod{2}\}$ . Collins *et al.* [37] defined the Mermin polynomials for general  $n$  pairs of single-particle ( $n$ -qubit) operators  $\{(a_l, a'_l) \mid l = 1, 2, \dots, n\}$  using the following recursive relations:

$$M_k = \frac{1}{2} M_{k-1} (a_k + a'_k) + \frac{1}{2} M'_{k-1} (a_k - a'_k), \quad (67a)$$

$$M'_k = \frac{1}{2} M'_{k-1} (a'_k + a_k) + \frac{1}{2} M_{k-1} (a'_k - a_k), \quad (67b)$$

where  $M_1 = a_1$  and  $M'_1 = a'_1$ . Note that  $M'_k$  is obtained by exchanging all the primed and non-primed  $a$ 's. Here, we define all  $a$  operators as  $n$ -qubit tensor products  $a_l = \mathbb{1} \otimes \dots \otimes \mathbb{1} \otimes a \otimes \mathbb{1} \otimes \dots \otimes \mathbb{1}$ , where  $a$  acts on the  $l$ -th qubit and similarly for primed  $a$ 's. Thus, we have  $[a_k, a_l] = 0$ ,  $[a'_k, a'_l] = 0$ , for all indices and  $[M_k, a_l] = 0$  and  $[M'_k, a'_l] = 0$  for  $k < l$ . Finally,  $a$  and  $a'$  are often assumed to be dichotomic (involution) operators:  $a_k^2 = a'^2_k = \mathbb{1}$  for all  $k$ .

To proceed, we rewrite Eq. (67) using the following matrix notation.

$$\begin{pmatrix} M_1 \\ M'_1 \end{pmatrix} = \begin{pmatrix} a_1 \\ a'_1 \end{pmatrix} = \frac{1}{2} \begin{pmatrix} a_1 + a'_1 & a_1 - a'_1 \\ -a_1 + a'_1 & a_1 + a'_1 \end{pmatrix} \begin{pmatrix} 1 \\ 1 \end{pmatrix}. \quad (68)$$

$$\begin{pmatrix} M_k \\ M'_k \end{pmatrix} = \frac{1}{2} \begin{pmatrix} a_k + a'_k & a_k - a'_k \\ -a_k + a'_k & a_k + a'_k \end{pmatrix} \begin{pmatrix} M_{k-1} \\ M'_{k-1} \end{pmatrix} \quad (69)$$

$$= \frac{1}{\sqrt{2}} \left( a_k e^{\frac{i\pi}{4} Y} + a'_k e^{-\frac{i\pi}{4} Y} \right) \begin{pmatrix} M_{k-1} \\ M'_{k-1} \end{pmatrix} \quad (70)$$

$$= \dots$$

$$= 2^{-\frac{k}{2}} \prod_{l=1}^k \left( a_l e^{\frac{i\pi}{4} Y} + a'_l e^{-\frac{i\pi}{4} Y} \right) \begin{pmatrix} 1 \\ 1 \end{pmatrix}, \quad (71)$$

where  $Y = \begin{pmatrix} 0 & -i \\ i & 0 \end{pmatrix}$  is the Pauli matrix acting on an ancilla qubit that encodes the algebraic recursive relation <sup>4</sup>. For convenience, we refer to the matrix operator

<sup>4</sup> Note that using the matrix form for  $Y$  does *not* mean we have chosen the computation basis for the system qubits

$\frac{1}{2} \begin{pmatrix} a_k + a'_k & a_k - a'_k \\ -a_k + a'_k & a_k + a'_k \end{pmatrix} = \frac{1}{\sqrt{2}} (a_k e^{\frac{i\pi}{4} Y} + a'_k e^{-\frac{i\pi}{4} Y}) \equiv \mathcal{A}_k$  as the transfer matrix.

The algebraic symmetry, derived from the interchange of all primed and non-primed  $a$ 's in Eq. (69), becomes more transparent when expressed in terms of symmetric and antisymmetric combinations. This transparency is achieved by transforming  $(M_k, M'_k)$  into  $\frac{1}{2}(M_k + M'_k, -M_k + M'_k) \equiv (M_k^+, M_k^-)$  through the left multiplication of  $\frac{1}{\sqrt{2}} e^{\frac{i\pi}{4} Y}$  on both sides of Eq. (69). Given that  $[\mathcal{A}_k, e^{\frac{i\pi}{4} Y}] = 0$ , the transfer matrix stays the same:  $\mathcal{A}_k = \frac{1}{\sqrt{2}} (a_k e^{\frac{i\pi}{4} Y} + a'_k e^{-\frac{i\pi}{4} Y}) = \mathbb{1} a_k^+ - iY a_k^-$ , where  $a_k^\pm = (\pm a_k + a'_k)/2$ . Then, the recursive formula becomes

$$\begin{pmatrix} M_1^+ \\ M_1^- \end{pmatrix} = \mathcal{A}_0 \begin{pmatrix} 1 \\ 0 \end{pmatrix}, \quad (72)$$

$$\begin{pmatrix} M_k^+ \\ M_k^- \end{pmatrix} = \mathcal{A}_k \begin{pmatrix} M_{k-1}^+ \\ M_{k-1}^- \end{pmatrix} \quad (73)$$

$$= (\mathbb{1} a_k^+ - iY a_k^-) \begin{pmatrix} M_{k-1}^+ \\ M_{k-1}^- \end{pmatrix} \quad (74)$$

$= \dots$

$$= \prod_{l=1}^k (\mathbb{1} a_l^+ - iY a_l^-) \begin{pmatrix} 1 \\ 0 \end{pmatrix}. \quad (75)$$

The  $\pm$  superscripts indicate the sign change under the symmetry of exchanging all the primed and non-primed  $a$ 's, so  $(M_l^+, M_l^-)^T \rightarrow (M_l^+, -M_l^-)^T = Z(M_l^+, M_l^-)^T$  and  $\mathcal{A}_k = \mathbb{1} a_k^+ - iY a_k^- \rightarrow \mathbb{1} a_k^+ + iY a_k^- = Z \mathcal{A}_k Z$ , where  $Z = \begin{pmatrix} 1 & 0 \\ 0 & -1 \end{pmatrix}$ . Thus, Eq. (74) still holds under the symmetry of exchanging all the primed and non-primed  $a$ 's as it should be.

First, we point out some similarity between Eq. (69) and the unitary operator  $\mathcal{U}$  in the boxed part in the circuit in Fig. 1 that is given by

$$\begin{aligned} \mathcal{U} &= H \otimes I \cdot \left( |0\rangle\langle 0|_a \otimes U + |1\rangle\langle 1|_a \otimes V \right) \cdot H \otimes I \\ &= |+\rangle\langle +|_a \otimes U + |-\rangle\langle -|_a \otimes V \\ &= \frac{1}{2} \begin{pmatrix} U + V & U - V \\ U - V & U + V \end{pmatrix}. \end{aligned} \quad (76)$$

The operators  $|\pm\rangle\langle \pm| = (\mathbb{1} \pm X)/2$  are both projection operators. Consequently,  $\mathcal{U}$  is unitary, satisfying the condition  $\mathcal{U}\mathcal{U}^\dagger = |+\rangle\langle +|_a \otimes (UU^\dagger) + |-\rangle\langle -|_a \otimes (VV^\dagger) = \mathbb{1}_a \otimes \mathbb{1}$ . In Eq. (69), the transfer matrix  $\mathcal{A}_k$  is similar to Eq. (76) except for the minus sign of the (2,1) matrix element. Due to this minus sign, this matrix operator is not unitary, so we need a second ancilla qubit to be used with the LCU for this matrix operator. The first ancilla deterministically encodes the mutual recursions and the second ancilla probabilistically block-encodes the non-unitary into a unitary via LCU and measurements. However, we can solve the recursion described in Eq. (75) in a closed form using the  $Y$  eigenbasis  $\{|+\rangle = \frac{1}{\sqrt{2}} \begin{pmatrix} 1 \\ i \end{pmatrix}, |-\rangle = \frac{1}{\sqrt{2}} \begin{pmatrix} 1 \\ -i \end{pmatrix}\}$  to preserve the first qubit. We plug the following resolution of identity

$$\begin{aligned} \mathbb{1} &= \frac{\mathbb{1} + Y}{2} + \frac{\mathbb{1} - Y}{2} \\ &= |+\rangle\langle +| + |-\rangle\langle -| = (|+\rangle \ |-\rangle) \begin{pmatrix} \langle +| \\ \langle -| \end{pmatrix} \end{aligned}$$

onto both sides of the product in Eq. (75), and find

$$\begin{aligned} \begin{pmatrix} M_k^+ \\ M_k^- \end{pmatrix} &= (|+\rangle \ |-\rangle) \begin{pmatrix} \langle +| \\ \langle -| \end{pmatrix} \prod_{l=1}^k \left[ (\mathbb{1} a_l^+ - iY a_l^-) (|+\rangle \ |-\rangle) \begin{pmatrix} \langle +| \\ \langle -| \end{pmatrix} \right] \begin{pmatrix} 1 \\ 0 \end{pmatrix} \\ &= (|+\rangle \ |-\rangle) \begin{pmatrix} \prod_{l=1}^k (a_l^+ - i a_l^-) & 0 \\ 0 & \prod_{l=1}^k (a_l^+ + i a_l^-) \end{pmatrix} \begin{pmatrix} \langle +| \\ \langle -| \end{pmatrix} \begin{pmatrix} 1 \\ 0 \end{pmatrix} \\ &= \frac{1}{\sqrt{2}} (|+\rangle \ |-\rangle) \begin{pmatrix} \prod_{l=1}^k (a_l^+ - i a_l^-) \\ \prod_{l=1}^k (a_l^+ + i a_l^-) \end{pmatrix} = \frac{1}{2} \begin{pmatrix} 1 & 1 \\ i & -i \end{pmatrix} \begin{pmatrix} \prod_{l=1}^k (a_l^+ - i a_l^-) \\ \prod_{l=1}^k (a_l^+ + i a_l^-) \end{pmatrix}. \end{aligned}$$

Therefore

$$\begin{pmatrix} M_k \\ M'_k \end{pmatrix} = \begin{pmatrix} 1 & -1 \\ 1 & 1 \end{pmatrix} \begin{pmatrix} M_k^+ \\ M_k^- \end{pmatrix} = \left( \frac{1-i}{2} \right)^{k+1} \begin{pmatrix} 1 & i \\ i & 1 \end{pmatrix} \begin{pmatrix} \prod_{l=1}^k (a_l^+ + i a_l) \\ \prod_{l=1}^k (a_l + i a_l') \end{pmatrix},$$

where we have used  $a_l^+ \pm i a_l^- = \frac{1 \mp i}{2} (a_l \pm i a_l')$ . The symmetry of exchanging all the primed and non-primed symbols is equivalent to swapping the two rows of the vectors  $(M_k, M'_k)^T$  and  $(\prod_{l=1}^k (a_l^+ + i a_l), \prod_{l=1}^k (a_l + i a_l'))^T$ , which is the action of  $X = \begin{pmatrix} 0 & 1 \\ 1 & 0 \end{pmatrix}$  operator. The recursive formula respects this symmetry because  $\begin{pmatrix} 1 & i \\ i & 1 \end{pmatrix}$  and  $X$  operator commute.

Therefore, we have the following closed-form expres-

sions for all  $M_k$  and  $M'_k$  defined the by the recursion in

Eq. (67).

$$M_k = \frac{(1-i)^{k+1}}{2^{k+1}} \left[ i \prod_{l=1}^k (a_l + ia'_l) + \prod_{l=1}^k (a'_l + ia_l) \right], \quad (77a)$$

$$M'_k = \frac{(1-i)^{k+1}}{2^{k+1}} \left[ \prod_{l=1}^k (a_l + ia'_l) + i \prod_{l=1}^k (a'_l + ia_l) \right]. \quad (77b)$$

With Eq. (77), we can easily write down the closed-form for the Svetlichny polynomial  $S_k$  defined in Ref. [37, Eq. (13)]. For  $k$  even,  $S_k$  takes an especially symmetric form as

$$S_k = \frac{(1-i)^k}{2^{k+1}} \left[ \prod_{l=1}^k (a_l + ia'_l) + \prod_{l=1}^k (a'_l + ia_l) \right]. \quad (78)$$

We can check Eq. (77a) for  $k = 3$  as follows.

$$\begin{aligned} M_3 &= \frac{(1-i)^4}{2^4} [i(a_1 + ia'_1)(a_2 + ia'_2)(a_3 + ia'_3) \\ &\quad + i^3(a_1 - ia'_1)(a_2 - ia'_2)(a_3 - ia'_3)] \\ &= \frac{-i}{4} [(a_1 + ia'_1)(a_2 + ia'_2)(a_3 + ia'_3) \\ &\quad - (a_1 - ia'_1)(a_2 - ia'_2)(a_3 - ia'_3)] \\ &= \frac{1}{2} (a'_1 a_2 a_3 + a_1 a'_2 a_3 + a_1 a_2 a'_3 - a'_1 a'_2 a'_3). \end{aligned}$$

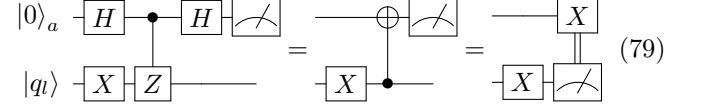
This result agrees with Eq. (5) in Ref. 37.

To measure  $M_k$  with the closed form of Eq. (77a), we can measure the two product terms separately. For each product term, we recursively implement each factor with LCU for the sum of two terms  $a_l$  and  $ia'_l$ . Thus, we only need one ancilla if we reuse and reset it in the iterative algorithm (in this specific case, reset is not necessary since the same LCU coefficients appear in all factors). The projective measurement on ancilla can also be re-interpreted as measurement on the qubit of main system as shown in Eq. (79). The two theoretical equivalent options (measure a single ancilla iteratively vs measure all qubits in the main entangled system) can be exploited to optimize readout error, post-selection cost, and maybe even avoid certain loopholes in quantum entanglement verification.

### 1. Mermin Polynomial Measurement equivalence

We choose the setting [38]  $a_l = \sigma_l^x$  and  $a'_l = \sigma_l^y$  for all qubits. The factors appearing in  $M_k$  takes the form of the ladder operators  $a_l \pm ia'_l = \sigma_l^x \pm i\sigma_l^y = \sigma_l^\pm$ , which is exactly the same factor appeared in the polynomial defined by Mermin [36, Eq. (2)]. With a slight change of notation, we write  $\sigma_l^x \pm i\sigma_l^y \equiv X_l \pm iY_l = \frac{1 \pm Z_l}{2} (2X_l)$ , where the non-unitary part  $U_\pm = \frac{1 \pm Z_l}{2}$  can be implemented using the circuit in Fig. 1. Considering the first term of  $U_\pm$  is the identity operator  $\mathbb{1}$ , we simplify the

circuit for  $U_\pm X_l$  as follows:



The equivalence between direct measurement on the principle system and indirect measurement on an environmental pointer state, represented by ancilla qubits above.

As a final brief note, recall the polynomial factorized as a sum over global products of  $\sigma_l^\pm = x$ . Along with  $\sigma_l^z$ , these operators serve a basis to construct correlation functions of spins  $\langle \Psi | \sigma_k^-(t) \sigma_l^+(0) | \Psi \rangle$  for example. By judiciously tracking fermionic phase factors we can promote this expression to  $\langle \Psi | c_k(t) c_l^\dagger(0) | \Psi \rangle$ . The synthesis techniques described above can be used to construct measurement gadgets for one- and two-point correlation functions—used in the natural sciences and high-rank polynomials moments as in the Mermin’s entanglement witness. A comprehensive application of symmetric considerations to efficient entanglement classification and manipulation via measurement is left as future work.

## IV. CONCLUSIONS AND DISCUSSION

We have introduced near term algorithms that utilize both product and sum formulas to probabilistically sample symmetric operators on quantum and classical computers.

As a first illustrative application, we examine a spectral random walk with stochastic dynamics that preserve time-reversal-invariance. We emphasize both symmetric and symmetry-breaking walks. A second application demonstrates how our protocol enhances the precision scaling of factorizing time evolution operators. By avoiding potential future amplitude amplifications, a characteristic feature of block encodings, we analyze trade-offs with respect to sample complexity and applications. We expect our algorithm to both inspire future advanced unitary operator synthesis while also finding practical applications in the near term due to straightforward nature. In the third application, we present a symmetry-enhanced variational form within the context of preparing eigenstates of a spin-chain. Lastly, our fourth application utilizes the intrinsic symmetries of Mermin-polynomials to provide a natural framework for efficient encoding and entanglement verification.

In a sense, our algorithm can be viewed as a simplified and less coherent alternative to qubitization [4]. We have traded coherences, which are typically used to boost transition probabilities to unity (implicitly required to construct deterministic algorithms), for accepting the outcomes of measurements which alleviates the need to laboriously amplify. This approach represents a somewhat reduced yet more readily attainable model of quantum computation. Despite this apparent trade-off, we nev-

ertheless find a wide variety of applications including spectral quantum walks, time evolution, variational state preparation, and entanglement verification. We expect further investigations of probabilistic symmetric forms will unravel additional applications, bridging the gaps between theoretical realizations, available resources, and practical implementations. In particular, investigating symmetric forms using Jordan products of Jordan products, which have been employed as estimates for Trotter products, has recently been demonstrated in certain Jordan algebraic settings [39].

## V. ACKNOWLEDGEMENTS

We thank Titus Morris for discussions and reviewing our manuscript. E.D. is supported by the U.S. Department of Energy, Office of Science, Advanced Scientific Research Program, Early Career Award under contract number 3ERKJ420. S.C. acknowledges DOE ASCR funding under the Quantum Computing Application Teams program, FWP No. ERKJ347. Y.W. is supported by the U.S. Department of Energy, Office of Science, National Quantum Information Science Research Centers, Quantum Science Center. This research used resources of the Oak Ridge Leadership Computing Facility, which is a DOE Office of Science User Facility supported under Contract DE-AC05-00OR22725.

## VI. AUTHOR DECLARATIONS

### Conflict of interest

The authors have no conflict of interest to disclose.

## VII. AUTHOR CONTRIBUTIONS

**Sarah Chehade:** Formalization of algorithm utilizing Jordan algebras in dynamical factorization. **Eugene Dumitrescu:** Conceptualization of the algorithm, dynamical and verification applications. **Yan Wang:** Further development of the ideas and methodology, numerical simulation, and visualization. All authors are involved in writing the original draft and reviewing and editing the final manuscript.

### Appendix A: Survival Probabilities for Quantum Zeno Effect

As given in the main text, after  $n$  measurements of ancilla with outcome 0's (denote the success probability of obtaining these 0 outcomes as  $P(0)$ ), the final survival probability  $S_n$  (conditioned on successfully measuring 0's on ancilla), i.e., measurement of  $\hat{O} = |\Psi\rangle\langle\Psi|$  in the principal system at the final state

$|\Phi\rangle = \cos^n(HT/n)|\Psi\rangle / [\langle\Psi|\cos^{2n}(HT/n)|\Psi\rangle]^{1/2}$  (denote  $HT = h$ ), is given by

$$S_n \equiv S_n(\Phi \rightarrow \Psi | 0) \quad (\text{A1})$$

$$= \text{Tr}\left(|\Phi\rangle\langle\Phi| \hat{O}\right) = |\langle\Psi|\Phi\rangle|^2 \quad (\text{A2})$$

$$= \frac{|\langle\Psi|\cos^n(HT/n)|\Psi\rangle|^2}{\langle\Psi|\cos^{2n}(HT/n)|\Psi\rangle} \quad (\text{A3})$$

$$= \frac{\left|\langle\Psi\left|1 - \frac{h^2}{2n} + \frac{h^4}{8n^2} + \mathcal{O}\left(\frac{1}{n^3}\right)|\Psi\rangle\right|^2}{\langle\Psi\left|1 - \frac{h^2}{n} + \frac{h^4}{2n^2} + \mathcal{O}\left(\frac{1}{n^3}\right)|\Psi\rangle}\right.} \quad (\text{A4})$$

$$= 1 - \frac{(\overline{h^2} - \overline{h^2})^2}{4n^2} + \mathcal{O}\left(\frac{1}{n^3}\right), \quad (\text{A5})$$

where  $\overline{\delta} = \langle\Psi|\delta|\Psi\rangle$ . Since  $P(0) = \langle\Psi|\cos^{2n}(HT/n)|\Psi\rangle$ , the survival probability of the entire system is given by

$$\check{S}_n \equiv S_n(\Phi \rightarrow \Psi \cap 0) \quad (\text{A6})$$

$$= S_n(\Phi \rightarrow \Psi | 0)P(0) = |\langle\Psi|\cos^n(HT/n)|\Psi\rangle|^2$$

$$= 1 - \frac{\overline{h^2}}{n} + \mathcal{O}\left(\frac{1}{n^2}\right).$$

Note that this is different from unconditioned (i.e., measuring the ancilla but without post-selection) survival probability of the principal system alone  $S_n(\Phi \rightarrow \Psi) = \sum_{k=0}^{2^n-1} S_n(\Phi \rightarrow \Psi | k)P(k)$  (the binary representation of  $k$  is the outcome string). Since  $1 \geq S_n(\Phi \rightarrow \Psi) \geq \check{S}_n \rightarrow 1$  at QZE measurement frequency limit,  $P(0 | \Phi \rightarrow \Psi) = \check{S}/S_n(\Phi \rightarrow \Psi) \rightarrow 1$ , meaning that simply measuring the ancilla fast enough without recording the outcome, if the principal system is stationary at the end, then QZE indicates the ancilla is stationary (with high probability) during the entire process.

For a textbook case of quantum Zeno effect (QZE), the measurement  $\hat{O} = |\Psi\rangle\langle\Psi|$  is performed at each step, so the state is evolved over a period  $T/n$  at each step, and the final survival probability is given by

$$\tilde{S}_n = \tilde{S}_1^n \quad (\text{A7})$$

$$= \left|\langle\Psi|e^{-iHT/n}|\Psi\rangle\right|^{2n} \quad (\text{A8})$$

$$= 1 - \frac{(\overline{h} - \overline{h})^2}{n} + \mathcal{O}\left(\frac{1}{n^2}\right). \quad (\text{A9})$$

Noting  $0 \leq \overline{(h - \overline{h})^2} = \overline{h^2} - \overline{h}^2 \leq \overline{h^2}$ , we find  $S_n \geq \tilde{S}_n \geq \check{S}_n$ . Higher survival rate means slower evolution under monitoring, i.e., stronger QZE. The principal part of our system shows stronger QZE than standard case, but when considered together with ancillary part, the result is similar to the standard case.

## Appendix B: Continuous Variable Ancilla Example

Consider Fig. 1 where the ancilla qubit is replaced by a continuous variable qumode. Then a controlled time evolution of the principal system  $H$  to ancillary CV mode:  $e^{-i\hat{x}\otimes Ht}$  and starting from the a state  $|0\rangle\otimes|\Psi\rangle$ , where  $|0\rangle$

is the CV vacuum state and  $|\Psi\rangle = \sum c_n |n\rangle$ . The reduced density operator  $\rho(t)$  upon tracing out the ancillary CV mode (i.e., measuring the ancillary but without “recording data”—in practice, it means doing multiple shots and constructing an ensemble of the projected states) is:

$$\rho(t) = \text{Tr}_a [e^{-i\hat{x}\otimes Ht}(|0\rangle\otimes|\Psi\rangle\langle 0|\otimes\langle\Psi|)e^{+i\hat{x}\otimes Ht}] \quad (\text{B1})$$

$$= \int_{-\infty}^{+\infty} dx \langle x|e^{-i\hat{x}\otimes Ht}(|0\rangle\otimes|\Psi\rangle\langle 0|\otimes\langle\Psi|)e^{+i\hat{x}\otimes Ht}|x\rangle \quad (\text{B2})$$

$$= \int_{-\infty}^{+\infty} dx |\langle x|0\rangle|^2 e^{-ixHt} |\Psi\rangle\langle\Psi| e^{+ixHt} \quad (\text{B3})$$

$$= \sqrt{\frac{2}{\pi}} \int_{-\infty}^{+\infty} dx e^{-2x^2} \left( \sum_k |c_k|^2 |k\rangle\langle k| + \sum_{n\neq m} e^{-ix(\omega_n-\omega_m)t} c_n c_m^* |n\rangle\langle m| \right) \quad (\text{B4})$$

$$= \sum_k |c_k|^2 |k\rangle\langle k| + \sqrt{\frac{2}{\pi}} \sum_{n\neq m} c_n c_m^* |n\rangle\langle m| \int_{-\infty}^{+\infty} dx e^{-2x^2 - ix(\omega_n-\omega_m)t} \quad (\text{B5})$$

$$= \sum_k |c_k|^2 |k\rangle\langle k| + \sum_{n\neq m} e^{-t^2(\omega_n-\omega_m)^2/8} c_n c_m^* |n\rangle\langle m| \quad (\text{B6})$$

$$\rightarrow \sum_k |c_k|^2 |k\rangle\langle k| \equiv \rho^d, \text{ as } t \rightarrow \infty. \quad (\text{B7})$$

For the single step scheme, instead of a fixed (small) time  $t$ , we can use a random  $t$  in different shots following a Gaussian distribution  $p(t) = e^{-t^2/\alpha}/\sqrt{\alpha\pi}$ , where  $\alpha > 0$  and  $\int_{-\infty}^{+\infty} p(t)dt = 1$ . The mean probability  $\mathbb{E}(P_{0\rightarrow 0}) =$

$$\int p(t) \langle\Psi|\cos^2(Ht)|\Psi\rangle dt = \frac{1}{2} + \frac{1}{2} \langle\Psi|e^{-\alpha H^2}|\Psi\rangle > \frac{1}{2} \text{ and } \mathbb{E}(P_{0\rightarrow 1}) = 1 - \mathbb{E}(P_{0\rightarrow 0}) < \mathbb{E}(P_{0\rightarrow 0}).$$

- 
- [1] A. M. Childs and N. Wiebe, Hamiltonian simulation using linear combinations of unitary operations, *Quantum Info. Comput.* **12**, 901 (2012).
- [2] G. H. Low and I. L. Chuang, Optimal Hamiltonian simulation by quantum signal processing, *Phys. Rev. Lett.* **118**, 010501 (2017).
- [3] Z. M. Rossi, V. M. Bastidas, W. J. Munro, and I. L. Chuang, Quantum signal processing with continuous variables (2023), [arXiv:2304.14383 \[quant-ph\]](https://arxiv.org/abs/2304.14383).
- [4] G. H. Low and I. L. Chuang, Hamiltonian simulation by qubitization, *Quantum* **3**, 163 (2019).
- [5] Z. Hu, R. Xia, and S. Kais, A quantum algorithm for evolving open quantum dynamics on quantum computing devices, *Sci. Rep.* **10**, 3301 (2020).
- [6] N. Suri, J. Barreto, S. Hadfield, N. Wiebe, F. Wudarski, and J. Marshall, Two-unitary decomposition algorithm and open quantum system simulation, *Quantum* **7**, 1002 (2023).
- [7] G. H. Low, V. Kliuchnikov, and N. Wiebe, Well-conditioned multiproduct Hamiltonian simulation (2019), [arXiv:1907.11679 \[quant-ph\]](https://arxiv.org/abs/1907.11679).
- [8] A. Carrera Vazquez, D. J. Egger, D. Ochsner, and S. Woerner, Well-conditioned multi-product formulas for hardware-friendly Hamiltonian simulation, *Quantum* **7**, 1067 (2023).
- [9] G. Rendon, J. Watkins, and N. Wiebe, Improved accuracy for Trotter simulations using Chebyshev interpolation (2022), [arXiv:2212.14144 \[quant-ph\]](https://arxiv.org/abs/2212.14144).
- [10] S. Zhuk, N. Robertson, and S. Bravyi, Trotter error bounds and dynamic multi-product formulas for Hamiltonian simulation (2023), [arXiv:2306.12569 \[quant-ph\]](https://arxiv.org/abs/2306.12569).
- [11] J. M. Martyn, Y. Liu, Z. E. Chin, and I. L. Chuang, Efficient fully-coherent quantum signal processing algorithms for real-time dynamics simulation, *J. Chem. Phys.* **158**, 024106 (2023).
- [12] H. F. Trotter, On the product of semi-groups of operators, *Proc. Amer. Math. Soc.* **10**, 545 (1959).
- [13] M. Suzuki, Generalized Trotter’s formula and systematic approximants of exponential operators and inner derivations with applications to many-body problems, *Commun. Math. Phys.* **51**, 183 (1976).
- [14] A. M. Childs, Y. Su, M. C. Tran, N. Wiebe, and S. Zhu, Theory of Trotter error with commutator scaling, *Phys. Rev. X* **11**, 011020 (2021).

- [15] J. Haah, M. B. Hastings, R. Kothari, and G. H. Low, Quantum algorithm for simulating real time evolution of lattice Hamiltonians, *SIAM J. Comput.* **0**, FOCS18-250 (2021).
- [16] J. Ostmeier, Optimised Trotter decompositions for classical and quantum computing, *J. Phys. A: Math. Theor.* **56**, 285303 (2023).
- [17] P. Zeng, J. Sun, L. Jiang, and Q. Zhao, Simple and high-precision Hamiltonian simulation by compensating Trotter error with linear combination of unitary operations (2022), [arXiv:2212.04566 \[quant-ph\]](https://arxiv.org/abs/2212.04566).
- [18] M. Suzuki, General theory of fractal path integrals with applications to many-body theories and statistical physics, *J. Math. Phys.* **32**, 400 (1991).
- [19] P. Jordan, Über eine Klasse nichtassoziativer hyperkomplexer Algebren, *Nachrichten von der Gesellschaft der Wissenschaften zu Göttingen, Mathematisch-Physikalische Klasse* **1932**, 569 (1932).
- [20] W. Magnus, On the exponential solution of differential equations for a linear operator, *Communications on pure and applied mathematics* **7**, 649 (1954).
- [21] K. Goldberg, The formal power series for  $\log e^x e^y$ , *Duke Mathematical Journal* **23**, 13 (1956).
- [22] A. Bonfiglioli and R. Fulci, *Topics in Noncommutative Algebra: The Theorem of Campbell, Baker, Hausdorff and Dynkin*, Lecture Notes in Mathematics (Springer Berlin, Heidelberg, 2012), p145, Lemma 3.26.
- [23] E. B. Dynkin, Selected papers of E. B. Dynkin with commentary (American Mathematical Society, 2000) Chap. Calculation of the coefficients in the Campbell-Hausdorff formula, pp. 31–35, originally published (in Russian) in *Doklady Akad. Nauk SSSR* **57**, 323–326 (1947).
- [24] A. Monras, A. Beige, and K. Wiesner, Hidden quantum Markov models and non-adaptive read-out of many-body states (2011), [arXiv:1002.2337 \[quant-ph\]](https://arxiv.org/abs/1002.2337).
- [25] D. Lacroix, E. A. Ruiz Guzman, and P. Siwach, Symmetry breaking/symmetry preserving circuits and symmetry restoration on quantum computers, *The European Physical Journal A* **59**, 3 (2023).
- [26] J. Novotný, G. Alber, and I. Jex, Random unitary dynamics of quantum networks, *Journal of Physics A: Mathematical and Theoretical* **42**, 282003 (2009).
- [27] Y. Ge, J. Tura, and J. I. Cirac, Faster ground state preparation and high-precision ground energy estimation with fewer qubits, *Journal of Mathematical Physics* **60**, 10.1063/1.5027484 (2019).
- [28] L. Lin and Y. Tong, Near-optimal ground state preparation, *Quantum* **4**, 372 (2020), [arXiv:2002.12508](https://arxiv.org/abs/2002.12508).
- [29] T. Keen, E. Dumitrescu, and Y. Wang, *Quantum algorithms for ground-state preparation and Green's function calculation* (2021), [arXiv:2112.05731](https://arxiv.org/abs/2112.05731).
- [30] D. A. Levin and Y. Peres, *Markov Chains and Mixing Times* (American Mathematical Society, Providence, Rhode Island, 2017).
- [31] N. Hatano and M. Suzuki, Finding exponential product formulas of higher orders, in *Quantum Annealing and Other Optimization Methods*, edited by A. Das and B. K. Chakrabarti (Springer Berlin Heidelberg, Berlin, Heidelberg, 2005) pp. 37–68.
- [32] J. Watrous, Quantum computational complexity (2008), [arXiv:0804.3401 \[quant-ph\]](https://arxiv.org/abs/0804.3401).
- [33] N. Schuch and F. Verstraete, Computational complexity of interacting electrons and fundamental limitations of density functional theory, *Nat. Phys.* **5**, 732 (2009).
- [34] D. Wecker, M. B. Hastings, and M. Troyer, Progress towards practical quantum variational algorithms, *Phys. Rev. A* **92**, 042303 (2015).
- [35] K. Seki, T. Shirakawa, and S. Yunoki, Symmetry-adapted variational quantum eigensolver, *Phys. Rev. A* **101**, 052340 (2020).
- [36] N. D. Mermin, Extreme quantum entanglement in a superposition of macroscopically distinct states, *Phys. Rev. Lett.* **65**, 1838 (1990).
- [37] D. Collins, N. Gisin, S. Popescu, D. Roberts, and V. Scarani, Bell-type inequalities to detect true n-body nonseparability, *Phys. Rev. Lett.* **88**, 170405 (2002).
- [38] D. Alsina and J. I. Latorre, Experimental test of mermin inequalities on a five-qubit quantum computer, *Phys. Rev. A* **94**, 012314 (2016).
- [39] S. Chehade, S. Wang, and Z. Wang, Suzuki type estimates for exponentiated sums and generalized lie-trotter formulas in jb-algebras, *Linear Algebra and its Applications* **680**, 156 (2024).